

**A COMPRESSION ANVIL BEAM TEST METHOD TO MEASURE THE ARREST FRACTURE TOUGHNESS OF SEMI-BRITTLE MATERIALS WITH SMALL SPECIMENS**—M. Y. He, G. R. Odette, and M. Hribernik (University of California)

**OBJECTIVE**

The objective of this work was to develop a compression anvil loaded double-chevron beam test method fracture toughness test method to measure the arrest fracture toughness of cleavage oriented single crystal iron and other semi-brittle materials, based on a comprehensive finite element analysis that was used to select an effective specimen geometry and to quantify the stress intensity factor.

**SUMMARY**

Our goal was to design a specimen and test procedure that allowed the measurement of cleavage arrest ( $K_{Ia}$ ) fracture toughness in very small oriented iron single crystals ( $< 10$  mm). This was accomplished by incorporating iron single crystal slices into composite specimens. The test method described here is based on compression loaded, double-anvil beam fracture specimen, illustrated in Fig. 1. Conceptually, slow, uniform compression ( $\sigma$ ) loading of a beam with a shallow fatigue starter crack (thick black line) in an double anvil fixture (shown in black) results in Poisson stresses normal to the crack faces, and elastic energy is released as the crack (thin black line) propagates. Composite specimens were fabricated by a sequence of diffusion bonding single crystal slices (light grey) to low alloy steel arms (darker grey), followed by a sequence of electro-discharge machining (EDM), fatiguing and final EDM to the pre-cracked bar configuration shown in Fig. 1. The mode I stress intensity factor (SIF),  $K_I$ , is a strong function of the crack depth ( $a/W$ ). The SIF first increases to a maximum at a small  $a/W$ , and subsequently decreases very rapidly approaching 0 as  $a/W$  goes to 0.9 or less. The test is carried out by gradually increasing  $\sigma$  to the point where the crack initiates at  $\sigma_c$  and propagates until it arrests at a lower SIF  $K_I = K_{Ia}$ , terminating a substantial pop-in jump.

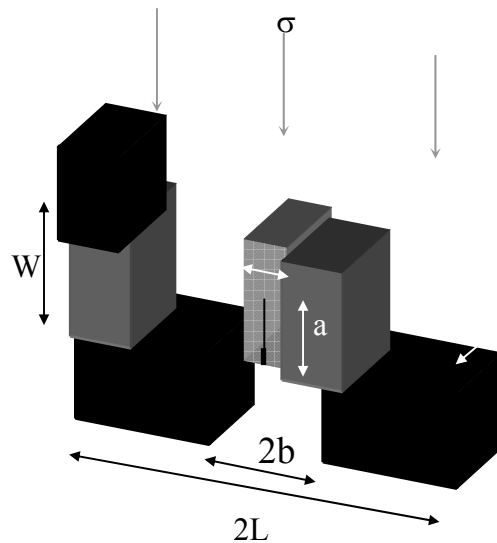


Fig. 1. A schematic perspective view of the compression loaded, double-anvil beam test fixture and specimen.

Implementation of this concept required an extensive finite element (FE) analysis, both to select an effective the specimen geometry, and quantify the SIF, in terms of its relation to the test parameters. In addition to the effects of varying specimen geometry, the FE analysis was used to examine the other factors such as friction effects, bi-material beams, composite beams, debonding and elasticity of the fixture. 4

This so-called compression anvil beam (CAB) test method was evaluated with tests on notched ( $\rho$ ) TiAl bars. The average initiation toughness  $K_{I_0} = 7.1 \pm 0.7 \text{ MPa}\sqrt{\text{m}}$  is consistent with previous measurements of the fracture toughness of TiAl, using fatigue cracked 3-point bend bars, of about  $K_{Ic} = 8 \pm 1 \text{ MPa}\sqrt{\text{m}}$  [10], as well as recent tests using a chevron notched, wedge loaded double cantilever beam (CWB) test method, described in a companion report in this semiannual [11], also yielding an average  $K_{Ic} = 7.1 \pm 1 \text{ MPa}\sqrt{\text{m}}$ . The corresponding  $K_{Ia}$  were 2.8 and 3.7  $\text{MPa}\sqrt{\text{m}}$  for the CAB and CWB tests, respectively. Note the CAB test method can also be applied to other brittle and semi-brittle materials

## PROGRESS AND STATUS

### Introduction

A convenient method to initiate a sharp precrack in brittle materials was introduced by Sadahiro [1] and Warren [2] for tungsten carbide and by Nose [3] for ceramics. This method involves initiating and arresting a pop-in crack from a shallow starter flaw, such as a hardness indent, by loading a beam specimen in compression as shown in Fig. 1. The method has been extended to a range of brittle materials [4-7], and incorporated in the ASTM Standard C1421-99 method for introducing pre-cracks in ceramic bend bars prior to fracture toughness testing [8]. Preliminary experiments have shown the effects of such test parameters as indentation load, anvil spacing and surface friction [1-3, 5, 7]. In addition, the stress intensity factor (SIF) as a function of crack length was determined by a finite element (FE) method [3]; however, some potentially invalid assumptions were made in this case regarding friction effects and the fixture-specimen geometry. A later FE analysis considered contact surface friction effects and the differences in the elastic properties of the specimen and fixture materials [5]. The present work builds upon these initial assessments and represents a comprehensive FE determination of the SIF, for the CAB test method. The effects of the anvil spacing, friction between upper and lower contact surfaces, as well as elastic deformation and geometry of the anvil, were examined. The stress intensities of a composite beam (see Fig. 1) made of materials with different elastic constants were also evaluated, as well as for specimens that experienced limited debonding.

### The Finite Element Model

An attractive feature of the bridge-indentation specimen is its ability to initiate and arrest a macroscopic cleavage crack over a very short distance. The test requires a shallow flaw at the center of the specimen bottom. The elastic energy release is provided by Poisson strains under compression loading. A shallow ( $a/W < 0.1$ ) crack first experiences an increasing SIF,  $K_I(a/W)$ , or energy release rate,  $J$ , that peaks at  $a/W \approx 0.1 - 0.2$ . The  $K_I$  decreases rapidly at higher  $a/W$  as the corresponding elastically strained volume of the material decreases. The crack arrests at  $K_I(a/W) = K_a$ . The  $K_I(a/W)$  is given by the standard SIF expression

$$K_I = Y_a(a,b,D,W,L)\sigma\sqrt{W} \quad (1)$$

Here,  $Y_a(a/W)$  is a non-dimensional SIF,  $K_I(a/W)/[\sigma\sqrt{W}]$ , for a specified specimen and anvil geometry including the crack length ( $a/W$ ), the anvil span ( $2b/W$ ) and height ( $D/W$ ), the beam length ( $2L/W$ ) where  $W$  is the width dimension. The SIF also depends on non-geometric effects, such as friction, represented by a coefficient  $\mu$ , and the elastic constants of the various test fixture and specimen materials. Thus development of the CAB test method required careful FE evaluation of  $Y_a(a/W)$ .

The Mode I SIF was analyzed by the FE method for the geometry shown in Fig. 2. The calculations were conducted using the general-purpose finite element code, ABAQUS. Only a half specimen was modeled (ABCD), due to symmetry considerations. One boundary condition involved applying a uniform vertical displacement,  $u_y$ , at the top surface (DC) of the specimen, which was allowed to slide on the anvil with the friction coefficient,  $\mu$ . The boundary at the top of the specimen was modeled for limiting friction free and no slip conditions. The specimen was modeled using a 40x50 rectangular mesh comprised of 2000 uniformly sized eight node isoparametric elements and 6506 nodes as shown in Fig. 2. The results for rigid anvil elements were compared to FE calculations for an elastic anvil, modeled using a uniformly sized 20x20 rectangular mesh. The whole mesh is comprised of 2400 eight node isoparametric elements 15

o ntaining 7462 nodes. The applied stress was found by averaging the compression/reaction force per unit area on the specimen top contact surface. A careful convergence study showed these meshes were sufficiently accurate to calculate the SIF. The energy release rate,  $J$ , was calculated by the domain integral method, for three to ten contours. The SIF is related to  $J$  as

$$K_I = \sqrt{[JE/(1- \nu^2)]} \quad (2)$$

Here  $E$  is the elastic modulus and  $\nu$  is Poisson's ratio.

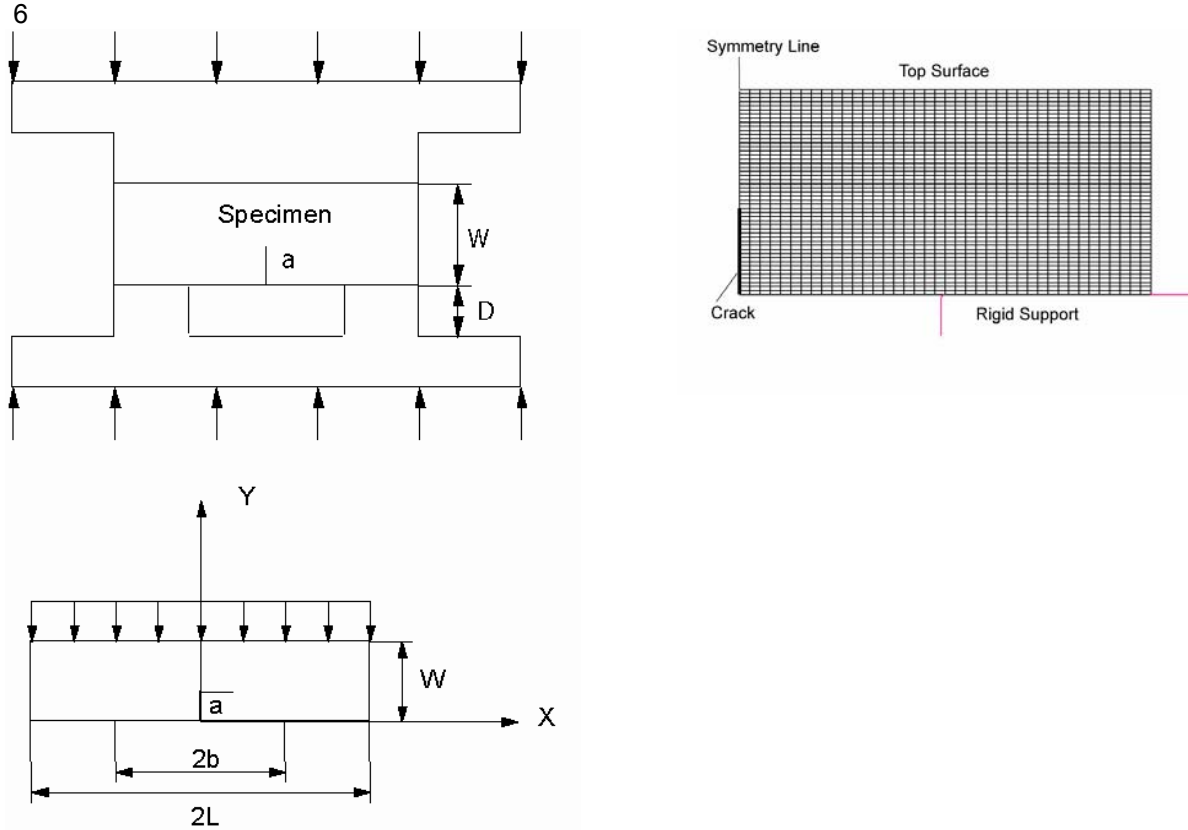


Fig. 2. A cross-section schematic view of specimen and load fixture, illustrating the key dimensions and the FE mesh.

The FE calculations for a particular specimen geometry and set of assumptions (like  $\mu$ ), represented by the normalized SIF curve,  $Y_a(a/W) = K_I/\sigma\sqrt{W}$ , are used to evaluate  $K_{Ia}$ . For example, assuming an arrest  $a_a/W = 0.74$ ,  $Y_a(0.74) = 0.06$ ,  $b/W = 0.5$ ,  $B/W = 0.5$ ,  $L/W = 1.15$ ,  $D/W = 0.5$ ,  $W = 7.7$  mm and pop-in load,  $P = 30,870$  N, gives  $\sigma_c = 452$  MPa and  $K_{Ia} = 2.4$  MPa $\sqrt{m}$ .

## Results

### Monolithic Specimen

The normalized SIF [ $Y_a(a/W) = K_I/(\sigma W^{1/2})$ ] for  $L/W = 1$  and  $D/W = 0.5$ , as a function of crack length,  $a/W$ , for rigid anvils spaced by  $b/W = 0.25, 0.5$  and  $1.0$ , assuming friction free contacts the specimen with both the lower anvils and upper pusher plate,  $\mu = 0$ , are shown in Fig. 3. The SIF reaches a maximum at  $a/W \approx 0.1$  to  $0.2$ , depending on  $b/W$ , and then decreases to zero as  $a/W$  approaches  $0.9$ . These results show that an anvil spacing of  $b/W = 0.5$  provides the largest SIF range in the crack initiation-arrest region, between  $a/W$  of about  $0.15$  to  $0.8$ . Except as otherwise noted, the FE computations described below will be for  $L/W = 1$ ,  $D/W = 0.5$ ,  $b/W = 0.5$ , rigid anvils and  $\mu = 0$ .

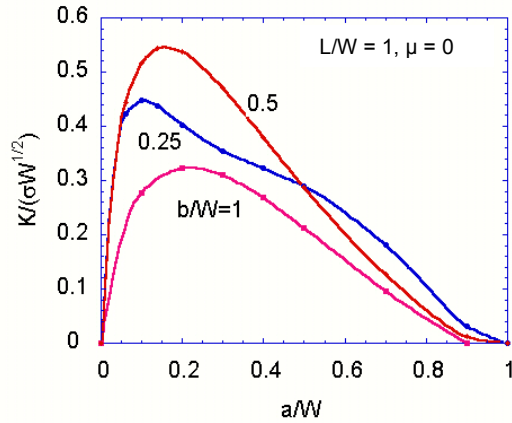


Fig. 3. The normalized SIF,  $Y_a(a/W) = K/(\sigma\sqrt{W})$ , as a function of the crack length  $a/W$  for  $L/W = 1$ ,  $b/W = 0.25, 0.5$ , and  $1.0$ , and  $\mu = 0$ .

The effect of friction between the specimen and anvil is shown in Fig. 4. Increasing  $\mu$  from 0 and 0.3 significantly reduces the SIF and shifts both the peak and post peak SIF curves to lower  $a/W$ . For example, the maximum SIF for  $\mu = 0.3$  is approximately one half of that for the  $\mu = 0$  case, and  $K_I$  approaches 0 at  $a/W = 0.4$ , versus 0.9 for the friction free conditions. These results assume the top surface is friction free. Figure 5 shows the limiting cases of friction free versus no slip conditions, when the specimen is not allowed to displace along its top surface, while  $\mu = 0$  for the specimen-anvil contact surface. The difference between these two limiting cases becomes increasingly significant for larger crack lengths at  $a/W > 0.3$ . Clearly it is important to minimize friction with the use of effective lubricants.

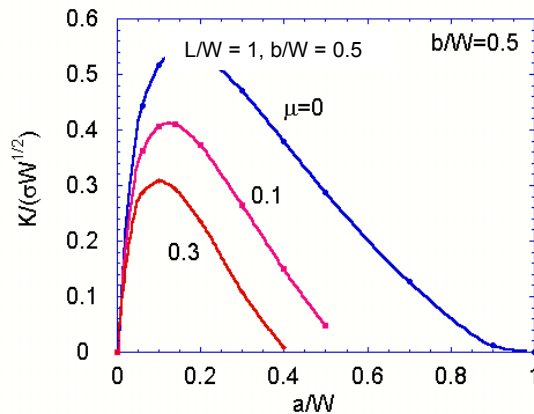


Fig. 4. The effects of the friction coefficient,  $\mu$ , between the specimen and anvil.

The normal ( $\sigma_{22}$ ) stress distributions, divided by the average applied stress ( $\sigma$ ) along the top surface of the specimen are shown in Fig. 6 for various crack lengths,  $\mu$  and  $b/W$ . The  $\sigma_{22}$  compressive stresses are not uniform, and increase from a minimum at the center ( $x/L = 0$ ) to a maximum at the edge ( $x/L = 1$ ). The uniformity of  $\sigma_{22}$  increases with decreasing  $a/W$  and  $b/W$  and increasing  $\mu$ .

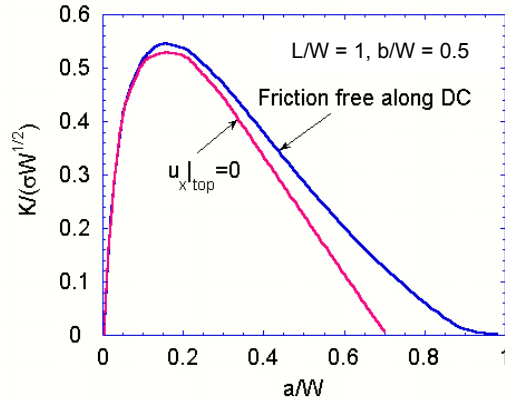


Fig. 5. The effects of the friction along the top contact surface for  $b/W = 0.5$ .

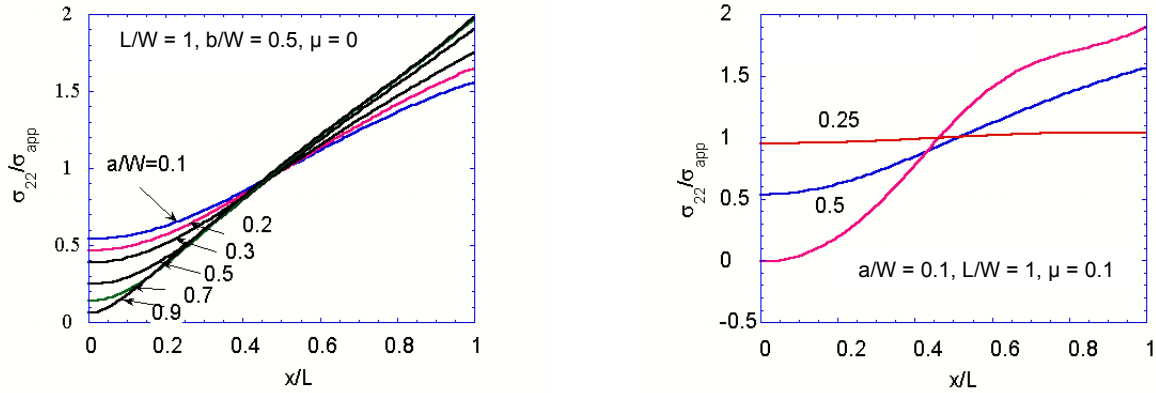


Fig. 6. The normal stress distributions along the top surface of the specimen for (a)  $L/W = 1$ ,  $b/W = 0.5$  and  $\mu = 0$ , and various  $a/W$ . (b). The corresponding normal stress distributions are shown for  $a/W = 0.1$  at  $b/W = 0.25, 0.5$ , and  $1.0$  and  $\mu = 0.1$ .

Figure 7 shows the effect of anvil stiffness on the SIF for two anvil heights,  $D/W = 0.5$  and  $3$ . The modulus for the anvil is taken as  $200$  GPa, the same as assumed for the modulus of steel, and  $\mu = 0$ . These results show that the effects of anvil elastic deformation are significant, even though the geometry of the anvil itself ( $D/W$ ) does not have a large effect. The assumption of a rigid support decreases the maximum SIF by about  $30\%$  compared to that for the elastic support.

### Bi-material Specimen

A bi-material specimen shown in Fig. 8 consists of bonded beams of brittle and ductile materials. The motivation for this specimen lies in the possibility of initiating a crack in the brittle material, such as a ceramic, and arresting the crack in a more ductile material, such as a single crystal iron. This case was analyzed with a modulus mismatch of  $E_1/E_2 = 2$ , for crack initiation in the more rigid, brittle material ( $E_1 = 340$  GPa). The normalized SIF is shown in Fig. 9 as a function of  $a/W$  for  $\mu = 0$ , and brittle to ductile layer thickness ratios of  $1/1$  (Fig. 9a) and  $1/9$  (Fig. 9b). The curve for a monolithic specimen ( $E = 170$  GPa) is shown for comparison. The stress intensity of the crack in the brittle material is about  $40\%$  higher than that for the monolithic specimen, roughly scaling with the square root of the local modulus for the layer that the crack lies in ( $E_L$ ), indicating that the total energy release rate is independent of the local  $E_L$  but scales

roughly with the rule of mixtures composite modulus  $[E_c = (W_1E_1 + W_2E_2)/(W_1 + W_2)]$ . Note, this evaluation did not consider the behavior of the crack at or in the interface itself, or effects such as residual stresses due to CTE mismatches or interface debonding.

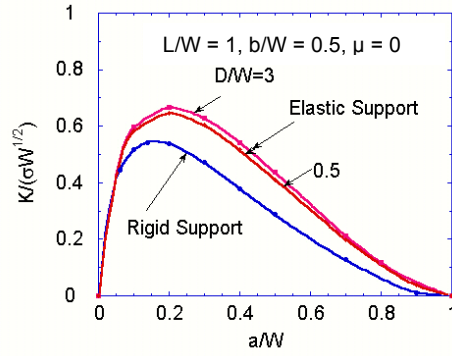


Fig. 7. The effects of anvil stiffness on stress intensity for  $D/W = 0.5$  and 3.

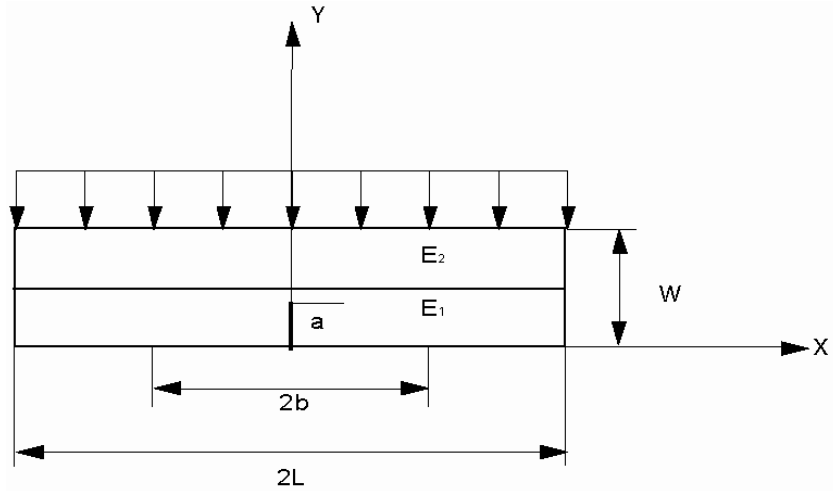


Fig. 8. Schematic of the bi-material specimen.

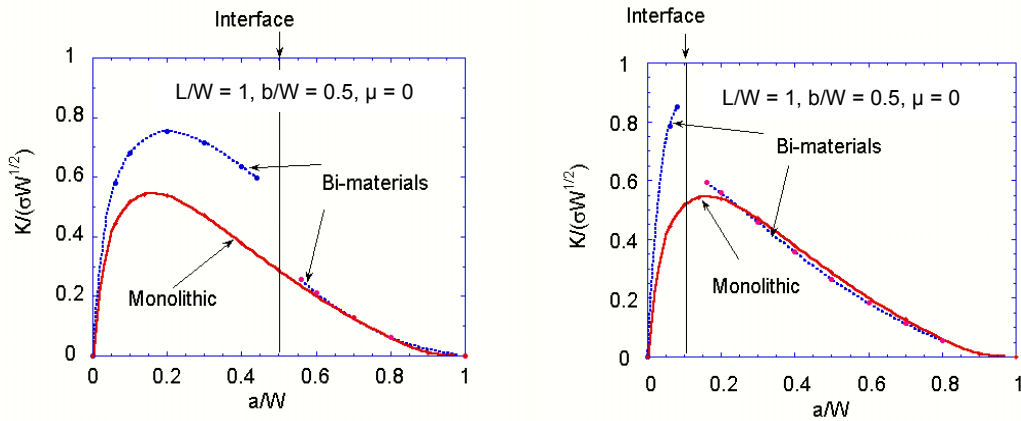


Fig. 9. The normalized SIF [ $K/(\sigma\sqrt{W})$ ] for the bi-material specimen with  $b/W = 0.5$ ,  $\mu = 0$ , and two interfacial positions (a)  $W_1/W = 0.5$  and (b)  $W_1/W = 0.1$ .

### Composite Beam Specimen

The composite beam specimen, shown in Fig. 10 is representative of a single crystal iron ( $E = 130$  GPa, for the  $\langle 100 \rangle$  directions along the beam axis) layer bonded between two polycrystalline steel sections ( $E = 200$  GPa). The motivation for this specimen configuration lies in the high cost and relatively small size of single crystal iron. The crack is intended to initiate and arrest entirely within the thin single crystal center section. The composite beam normalized SIF [ $K/(\sigma\sqrt{W})$ ] is shown in Fig. 11 as a function of  $a/W$ . Figure 11a shows the SIF for  $b/W = 0.5$ , a center section thickness  $h/W = 0.1$ , and  $\mu = 0$  in. The results for monolithic specimen with the same geometry are also included in Fig. 11a for comparison. Incorporating the single crystal section lowers the SIF approximately 24% compared to the Monolithic specimen. However, this is almost entirely due to the local  $E_L$  used to convert  $J$  to  $K_I$ , where  $E_L = 130$  GPa for the iron single crystal and 200 GPa for the polycrystalline steel. Thus the overall  $J$  is not sensitive to the local modulus. In contrast, Fig. 11a shows that both the  $J$  and the SIF decrease with increasing  $L/W$ . A stout  $L/W = 1$  provides the most effective CAB specimen geometry. Figure 11b shows a minor SIF decrease with increases in  $h/W$  from 0.1 to 0.2. Again, this is due to the effect of a higher rule of mixtures composite modulus,  $E_c$ , associated with the larger  $h/W$  that results in a decrease in  $J$ .

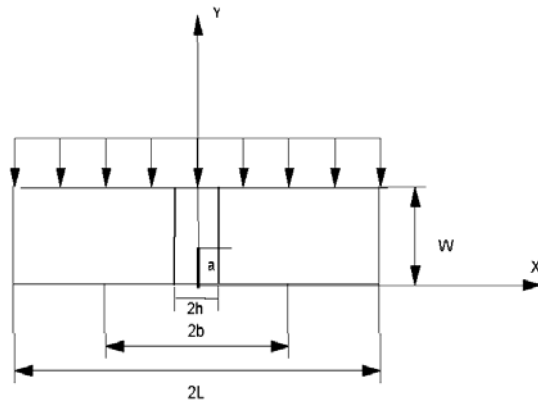


Fig. 10. Schematic of the composite beam specimen.

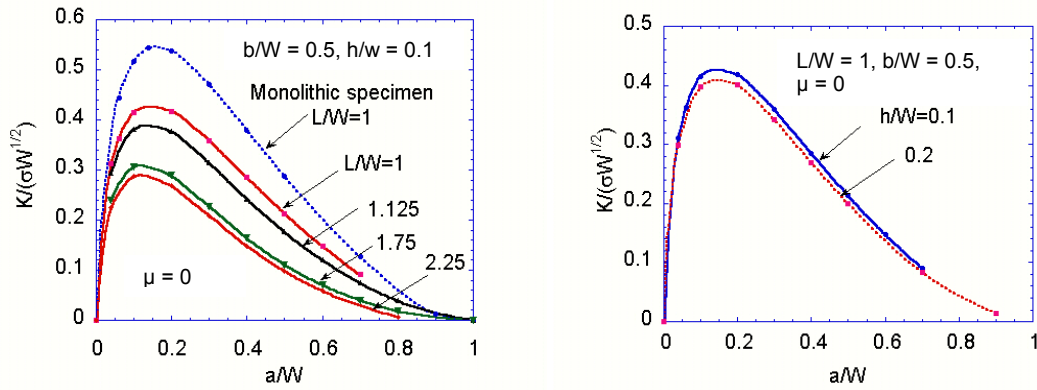


Fig. 11. The normalized stress intensity factor,  $K/(\sigma\sqrt{W})$ , for the sandwich specimen, (a) for a specimen with  $b/W = 0.5$ ,  $h/W = 0.1$ , and  $L/W = 1-2.25$ , (b) effects of the center section thickness,  $h/w = 0.1-0.2$ .

The composite steel-iron single crystal specimens have been observed to undergo limited interface debonding in some cases. This initially occurs during fatigue precracking and may be followed by additional interface crack growth to a depth,  $a_2$ , during compression anvil loading. The effects of the debonding on  $K_I$  for the main crack are shown in Fig. 12. Figure 12a shows that the interface cracks on both sides of length  $a_2/W$  result in shifts in the initial portion of the  $Y_a(a/W)$  SIF curves to higher  $a/W$  but has little effect beyond the peak. The peak SIF position increases roughly as  $a_2/W + 0.1$ . Thus these results show that if  $a_2$  is significantly less than the arrested crack length  $a_a$ , the effects of interfacial cracks are negligible. Figure 12b shows the effect of  $a_2/W$  on the non-dimensional energy release rate ( $JE/\sigma^2W$ ) for both the main crack at  $a/W = 0.7$ , and the interface crack itself. The energy release rate for the main crack is independent of  $a_2/W$  at a typical arrest depth, while the corresponding energy release rate for the interface crack is much lower and decreases with  $a_2/W$ . These result suggests that, if formed, interface debonding cracks will arrest at much shallower depths that the main crack, and thus will have little influence on the measured value of  $K_{Ia}$ .

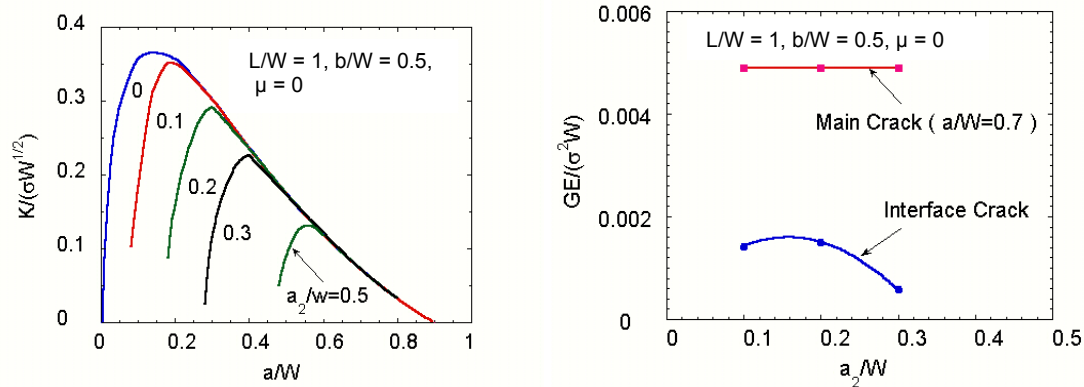


Fig. 12. (a) Effects of the interfacial crack length ( $a_2$ ) on the stress intensity factor of the main crack. (b) Stress intensity of the main crack at  $a/W = 0.7$  and the interface cracks versus  $a_2/W$ .

The FE results in this section can be summarized as follows.

- An effective geometry for shallow precracked CAB specimens is  $L/W = 1$ ,  $b/W = 0.5$ .
- The SIF are not sensitive to  $h/W$ ,  $D/W$  and limited interface debonding.

- The SIF are sensitive to friction effects, especially between the CAB specimen and anvil. Higher  $\mu$  decreases the  $K_I$ . Uncertainties about friction effects contribute the largest uncertainty to SIF and to the corresponding evaluations of  $K_{Ia}$ .
- The SIF are sensitive to the elasticity of the anvils, so this effect, which also reduces the  $K_I$ , must be properly accounted for.
- The SIF depend on the elastic modulus, and the effects of moduli in bimaterial and composite beam specimens affect  $K_I$ . Fortunately, the SIF roughly scales with  $\sqrt{(E_l/E_c)}$ , where  $E_l$  is the local elastic modulus and  $E_c$  is the rule of mixtures composite modulus.

#### Evaluation and Implementation of the CAB Test Method

The FE determination of the SIF was evaluated by static tests on 14 monolithic  $\gamma$ -TiAl specimens at room temperature [9]. The  $K_{Ic}$  and  $K_{Ia}$  tests were performed on electro-discharge machined (EDM) TiAl bars with dimensions of 4 x 8 x 18 mm, on a compression anvil fixture with  $L/W = 1$ ,  $b/W = 0.5$  and  $D/W = 0.5$ . A shallow half round notch  $\approx 0.1$  mm ( $a_i/W \approx 0.05$ ) in depth was EDM at the center of the bottom of the specimen to act as the crack initiating flaw, eliminating the potential effects of indentation load. However, the notch is not a sharp crack, so the initiation toughness is actually  $K_{Ip}$ . Thus there could be an effect of the notch root radius of  $\rho \approx 50$   $\mu$ m on the measured toughness. Nevertheless,  $K_{Ip}$  may be approximately equal  $K_{Ic}$  for the semi-brittle TiAl intermetallic alloy. The upper pusher plate was a polished  $Si_3N_4$  plate and the anvils were hardened tool steel. Lubrication of the contact surfaces between both the top pusher plate and the specimen and the bottom anvils and the specimen was provided by graphite powder. The specimens were loaded at a rate of 0.42  $\mu$ m/s on a servo-hydraulic MTS load frame until a pop-in was detected by both an acoustic emission sensor and a crack gauge glued on the specimen. Due to the low compliance of the rigid, compressively stressed system, a load drop does not occur at crack initiation at the critical applied compressive fracture stress,  $\sigma_c$ . The final arrest  $a_a/W$  was measured after the specimen was broken under four-point bending. The  $a_a/W$ ,  $a_i/W = 0.05$  and  $\sigma_c$  were used to determine the  $K_{Ip}$  and  $K_{Ia}$  based on the SIF [ $Y_a(a/W) = K_I/(\sigma\sqrt{W})$ ], derived from the FE analysis, the compression anvil dimensions cited above, assuming elastic anvils, frictionless contact surfaces with  $\mu = 0$ , and a TiAl modulus  $E = 170$  GPa.

The measured  $K_{Ip}$  and  $K_{Ia}$  results shown in Fig. 13 give an average  $K_{Ip} = 7.1 \pm 0.7$  MPa $\sqrt{m}$  and  $K_{Ia} = 2.8 \pm 1.4$  MPa $\sqrt{m}$ . The initiation  $K_{Ip}$  value is in reasonable agreement with the initiation toughness for static tests on fatigue precracked TiAl three point bend specimens of  $K_{Ic} \approx 8 \pm 1$  MPa $\sqrt{m}$  [10]. This average is also consistent with the average  $K_{Ic} = 7.1 \pm 1$  MPa $\sqrt{m}$  for the CAB specimens containing the sharp pop-in precracks tested under 4-point bending at dynamic loading rates of about 1000 MPa $\sqrt{m/s}$  [9]. Finally, the  $K_{Ip}$  is also identical to the average measured  $K_{Ic} = 7.1 \pm 1$  MPa $\sqrt{m}$  for TiAl chevron notched wedge loaded, double cantilever beam (CWB) specimens. The corresponding  $K_{Ia}$  for the CWB tests on TiAl was  $3.7 \pm 0.4$  MPa $\sqrt{m}$ .

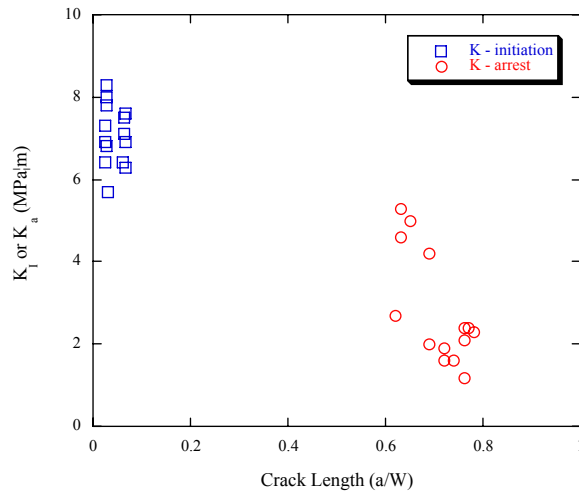


Fig. 13. Initiation and arrest toughness values at room temperature for TiAl evaluated through the finite element analysis of the single-edge notched-beam specimen.

#### Summary Discussion and Concluding Remarks

A compression loaded, double-anvil beam (CAB) test method has been developed to measure the crack arrest fracture toughness ( $K_{Ia}$ ) of cleavage oriented single crystal Fe and other semi-brittle materials using very small composite specimens that can be fabricated using minimal amounts of critical materials. This report focuses on finite element (FE) calculations that were used to select a specimen geometry that is appropriate, and to quantify the stress intensity factor (SIF) for the CAB specimen. An effective geometry to facilitate initiation and arrest events was found to be a total beam length on the anvils,  $2L/W = 2$ , and an anvil span,  $2b/W = 1$ . The SIF for the CAB specimen geometry first increases, and then decreases rapidly, with increasing  $a/W$  between 0 to 1. Thus crack initiation and arrest are manifested as a significant pop-in event. The FE solutions for normalized provide the SIF,  $[Y_a(a/W) = KI/\sigma\sqrt{W}]$ , to evaluate  $K_{Ia}$  based on the specimen-fixture geometry, the critical stress at crack initiation ( $\sigma_c$ ) and the crack depth at initiation ( $a_i/W$ ) and arrest ( $a_a/W$ ).

Implementation of the CAB test method was carried out using a double anvil fixture loaded on a MTS servohydraulic test frame. The test was instrumented with a crack gauge and acoustic emission sensor to detect crack initiation and  $\sigma_c$ . Evaluation of the CAB method was carried out by tests on TiAl specimens,

Caution must be used in using the CAB test to measure initiation toughness ( $K_{Ic}$ ) for specimens with sharp cracks. While, as noted previously, the CAB technique appears to work well for the initiation of a crack from a shallow starter notch in the TiAl tests at room temperature, other issues are encountered in CAB tests of composite specimens containing iron single crystals. In this case, a shallow fatigue crack is grown to provide a favorable initiation site. However, the fatigue cracks tend to be slanted in their preferred growth direction, and the cyclic loading generates dislocation structures in very soft single crystal iron that might affect the magnitude of  $K_{Ic}$ . For example, static CAB tests at  $-196^\circ\text{C}$  give an average  $K_{Ic} = 12.5 \pm 2.7 \text{ MPa}\sqrt{\text{m}}$ . This compares well with a corresponding values of  $11.4 \pm 3.8$  measured by CWB tests, but is much higher than the  $5.8 \pm 0.6 \text{ MPa}\sqrt{\text{m}}$  measured in static sharp pop-in crack 4-point bend tests. Indeed, the difficulty of initiating propagation from fatigue cracks represents a major limitation of the CAB test method, at least to measure  $K_{Ia}$  in single crystal Fe. The high effective values of  $K_{Ic}$  for the composite single crystal Fe specimens resulted in an effective upper temperature limit for the CAB tests of about  $-100^\circ\text{C}$ . At higher temperature the  $\sigma_c$  increased to the point where it resulted in deformation of the low alloy steel arms of the composite beams.

The largest uncertainty in the  $K_{Ia}$  measurements is the effects of friction. While the experimental procedure involved the use of graphite powder as a lubricant between the specimen and anvil and pusher surfaces, the neglect of possible friction effects may result in an overestimate of  $K_{Ia}$  in the CAB tests. There is not an independent calibration material for measuring  $K_{Ia}$  with the CAB test. However, it is notable that the  $K_{Ia}$  in single crystal Fe measured with the CWB and CAB tests were very consistent with one another [11]. For example at  $-196^{\circ}\text{C}$  the  $K_{Ia}$  was  $3.34 \pm 1.15$  and  $3.54 \pm 0.6$   $\text{MPa}\sqrt{\text{m}}$  for the CAB and CWB tests, respectively.

In summary, CAB tests on polycrystalline TiAl and single crystal Fe were successfully carried out using very small specimens with length, width and thickness dimensions of about  $16 \times 8 \times 4$  mm. Thus the CAB test method, including the use of composite specimens, offers a powerful new tool to measure the fracture toughness of brittle and semi-brittle materials, especially when specimen sizes and or the availability of materials are an issue.

### Future Work

The CAB and CWB test methods have been used to very successfully characterize the  $K_{Ia}$  in cleavage oriented iron single crystals, between  $-196$  and  $0^{\circ}\text{C}$  [5]. The resulting database is unique and has, for the first time, clarified the fundamental dynamics and controlling mechanisms of cleavage fracture. This database has also been used to develop a preliminary, but powerful, new semiempirical multiscale model of the macroscopic  $K_{Ic}(T)$  curve for complex structural steels. Notably, this model predicts an approximately invariant shape of the master toughness-temperature curve for complex steels, as well as the reference temperature shifts in the master curve due to irradiation hardening, that are in agreement with observation. Further analysis of the database and development of the model as well as full documentation of these results, including preparation of manuscripts for journal publication, will be completed during this current reporting period.

### **References**

- [1] T. Sadahiro and S. Takatsu, A new precracking method for fracture toughness testing of cemented carbides, in H. H. Hause et al. (eds.), *Modern Development in Power Metallurgy*, Vol. 14, Metal Powder Industries Federation, Princeton, N.J. (1981) 561.
- [2] R. Warren and B. Johannesson, Creation of stable cracks in hard metals using bridge indentation, *Powder Metall.* 27-1 (1984) 25.
- [3] T. Nose and T. Fujii, Evaluation of fracture-toughness for ceramic materials by a single-edge-precracked-beam method, *J. Am. Ceram. Soc.* 71-5 (1988) 328.
- [4] M. Y. He, H. C. Cao, and A. G. Evans, Mixed-mode fracture: The four-point shear specimen, *Acta Metall. Mater.* 38-5 (1990) 839.
- [5] J. L. Lue and R. O. Scattergood, Analysis of bridge-indentation precracking, *J. Hard Mater.* 6-1 (1995) 27.
- [6] A. K. Ray, A new technique for precracking ceramic specimens in fatigue and fracture, *J. Eur. Ceram. Soc.* 18-12 (1998) 1655.
- [7] I. Bar-On, J. T. Beals, G. L. Leatherman, and C. M. Murray, Fracture toughness of ceramic precracked bend bars, *J. Am. Ceram. Soc.* 73-81 (1990) 2519.
- [8] ASTM Standard C 1421-99, Standard Test Method for Determination of Fracture Toughness of Advanced Ceramics at Ambient Temperature, ASTM (1999).
- [9] M. L. Hribernik, Cleavage oriented iron single crystal fracture toughness, Ph.D. thesis, University of California, Santa Barbara (2006).
- [10] G. R. Odette, B. L. Chao, J. W. Sheckherd, and G. E. Lucas, Ductile phase toughening mechanisms in a TiAl-TiNb laminate composite, *Acta Metall. Mater.* 40 (1992) 2381.
- [11] G. R. Odette, M. Y. He, and M. L. Hribernik, A chevron notched wedge loaded double cantilever beam test method to measure the initiation and arrest fracture toughness of semi-brittle materials with small specimens, Fusion Materials Semiannual Progress Report for the Period Ending June 30, 2007, DOE-ER-0313/42.